Metal only Multi-beam Fabry-Perot Antenna

Jorge Ruiz-Garcia, Christos Bilitos, Enrica Martini, Giovanni Toso, Stefano Maci, David Gonzalez-Ovejero

Metal-only Multi-beam Fabry-Perot Antenna

Jorge Ruiz-García*, Christos Bilitos*, Enrica Martini†, Giovanni Toso‡,
Stefano Maci†, David González-Ovejero*
*Univ Rennes, CNRS: Institut d'Électronique et de Télécommunications de Rennes (IETR), UMR 6164,
35000 Rennes, France, {jorge.ruiz, david.gonzalez-ovejero}@univ-rennes1.fr
†University of Siena: Department of Information Engineering and Mathematics, 53100 Siena, Italy, macis@dii.unisi.it
‡European Space Agency - ESA/ESTEC: Radio Frequency Payloads & Technology Division, Noordwijk, The Netherlands.

***Abstract*—This paper presents a Fabry-Perot (FP) antenna with azimuthal scanning by beam switching at Ka-band. The system is composed of two stacked layers with circular shape. The bottom layer contains a Reflecting Luneburg Lens (RLL), which serves to generate a plane wave in the top one. In turn, the top layer hosts a Fabry-Perot cavity, which is used to gradually radiate the excited plane wave through a partially reflective surface (PRS), thus, producing a directive beam. Both the RLL and the FP cavity are azimuthally symmetric and allow one to generate identical pencil beams for any azimuthal direction. Moreover, it is possible to scan also in elevation by varying the height of the FP cavity, which provides 2D beam-steering capability. The double-layer approach guarantees the compactness of the device, whereas a full-metal implementation minimizes the propagation losses and renders the structure robust and fit for operation in harsh environments. The proposed system is well-suited for spatial applications, in particular for medium and high-gain antennas integrated in SmallSats and CubeSats.**

***Index Terms*—Fabry-Perot cavity, partially reflective surfaces (PRS), metasurfaces, Luneburg lens, beam-steering.**

I. Introduction

Space antennas are often required to provide high-gain while preserving a low profile and presenting low losses. Moreover, on-orbit beam-steering is also desirable for directed beam data transfer from the satellite to the ground stations. Classical solutions for beam steering high-gain antennas include reflectors mounted on rotating platforms [1] and phased arrays [2], but their size, weight and power consumption may not fit the conditions for new generation of satellite constellations and small satellites [3]. Other solutions consist in modulated metasurface (MTS) antennas [4]–[6] or compact beam-formers combined with slot arrays [7] which have been used to obtain multiple beams and can achieve scanning by beam switching. Although the later solutions fulfill the high-directivity and low-profile requirements, the azimuthal scanning range is limited. An interesting approach to obtain continuous beam-scanning consists in using in-plane mechanical rotation with planar structures, such as Risley prisms [8] or variable inclination continuous transverse stubs (VICTSs) [9]. The former is bulkier due to the stack of the two prisms, whereas the later presents a lower profile. Nonetheless, the in-plane rotation still entails a non-negligible complexity.

To avoid the aforementioned hurdles, peripherally excited (PEX) phased arrays [10] and Reflecting Luneburg Lenses (RLLs) [11] are very promising routes to explore. In both cases, a plane wave with arbitrary azimuthal direction can be generated in a parallel plate waveguide (PPW) using a limited number of ports. A PEX array requires a complex control network to tune the amplitude and phase of its ports, whereas RLLs are purely passive structures. A compact metal-only high-gain antenna based on a RLL beam-former was proposed in [11]. The antenna consists of a two-layer structure, where the RLL beam-former is integrated in the bottom PPW, whilst a modulated MTS antenna in the top layer acts as a radiating structure. A pencil-beam is efficiently generated and one can scan in azimuth (ϕ) and elevation (θ) by port switching. Nevertheless, the direction of the radiated beam in both ϕ and θ is defined by the relative angle between the direction of the generated plane wave (given by the activated port) and the direction of the MTS modulation in the top part. Thus, a change in azimuth also modifies the elevation direction and one cannot control independently the two angles. Furthermore, when the aforementioned relative incidence angle is too oblique the beam degrades significantly. Although both these effects can be corrected by rotating the upper layer according to the source position, so as to eliminate the elevation scanning, the inclusion of the rotation mechanism increases the system complexity.

To overcome these limitations, we propose the structure depicted in Fig. 1a, which uses a Fabry-Perot (FP) cavity with a partially reflective surface (PRS) as radiating aperture [12]. The plane wave generated by the RLL is coupled to the FP cavity laterally, as shown in Fig. 1b. The operating principle resembles that of a perforated PPW in cavity antennas [13]. In our configuration, the FP cavity presents full azimuthal symmetry, perfectly matching the RLL geometry. Hence, it is possible to radiate identical pencil beams for any azimuthal direction, given by the position of the port. One can also scan in elevation by modifying the height of the FP cavity. Therefore, by combining source switching (see sources in the inner circular region of the RLL in Fig. 1a) and the FP height variation, ϕ and θ can be controlled independently. The two-layer approach constitutes a low-profile architecture and, since we present a fully metallic implementation, the final structure is also robust and well-suited for operation in harsh environments [14]. Moreover, dielectric losses are avoided, maximizing then the radiation efficiency. The antenna operates in the Ka-band, with a central frequency $f_0 = 30$ GHz, and covers the fixed-satellite and mobile-satellite band for Earth-

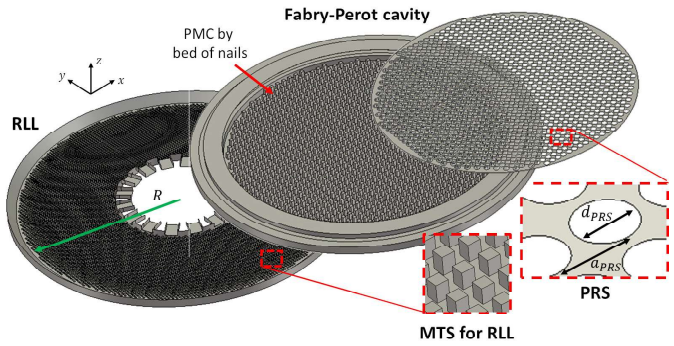

(a)

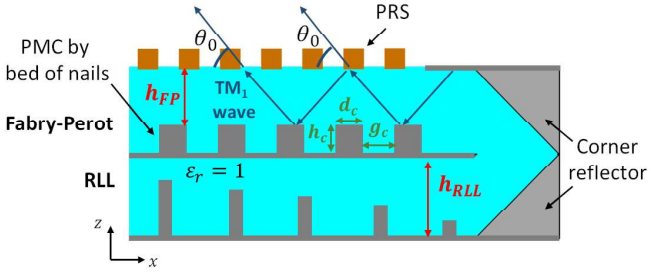

(b)

Fig. 1. (a) Metal-only antenna integrating the RLL and the FP cavity. The insets show the details of the modulated MTS implementing the RLL and the PRS on the FP topmost plate (the hole diameter $d_{PRS} = 2.55$ mm and the unit-cell periodicity $a_{PRS} = 3.1$ mm are indicated). (b) Section view and operating principle of the proposed structure, with the RLL in the bottom PPW and the FP cavity in the top layer.

to-space services $f \in [28, 32]$ GHz [15].

The paper is organized as follows. Section II describes the design of the Fabry-Perot cavity, and the needed modifications in the Reflecting Luneburg Lens to adapt it to the radiation aperture are discussed in Section III. The implementation of the antenna and the full-wave simulation results are presented in Section IV. Finally, we address the conclusions in Section V.

II. Fabry-Perot Cavity

As previously discussed, one of the main advantages of using a FP cavity as a radiating aperture is its azimuthal symmetry. That is, the angle of the beam in elevation does not change with the position of the port in the bottom PPW (see ports configuration of RLL in Fig. 1a). The operating principle illustrated in Fig. 1b is succinctly described in the following. In a nutshell, we exploit the TM_1 mode in the air-filled FP cavity that is formed by the perfect magnetic conductor (PMC) plane (bed of nails in Fig. 1) and a PRS placed at the topmost plate [12]. The latter allows for the plane TM_1 wave to be gradually radiated.

The main reason of including the PMC plane is that the corner reflector and PPW sections between the RLL and the FP (see Fig. 1b) cause the excitation of the TEM (or TM_0) mode, which produces an undesired end-fire lobe. Nonetheless, it is possible to suppress the fundamental mode by using a PMC ground for the FP cavity, which has been implemented by a bed of nails of constant height ($h_c = 2.8$ mm, $d_c = 1.4$ mm and $g_c = 1.9$ mm in Fig. 1b). This way, an equivalent PMC layer is seen by the traveling wave such that the TEM mode cannot propagate. Since the phase velocity of the plane TM wave is greater than the speed of light in the cavity, the phase constant in the FP region β_{FP} is smaller than the free space wavenumber k_0. We can readily obtain an approximation of the target β_{FP} through the expression $\sin\theta_0 = \beta_{FP}/k_0$, where θ_0 is the specified pointing angle in elevation. If we denote by $n_1 = \beta_{FP}/k_0 = \sin\theta_0$ the equivalent refractive index in the FP and as $n_0 = 1$ the one in the free-space, we have then that $n_1 < n_0$.

III. Modified Reflecting Luneburg Lens

A RLL is used to collimate the beam launched by a primary feed in the lower PPW and to generate a TM_1 mode with planar wavefront in the upper layer. The bottom PPW can be loaded with metallic posts of variable height to implement the needed refractive index profile n_{eq}, which has the closed-form expression given in eq. 17, [11]. The minimum achievable value of n_{eq} using the metallic pin graded index (GRIN) medium is 1, so that a discontinuity in the refractive index is unavoidable between the periphery of the RLL and the FP cavity. Since $n_0 = 1$ at the rim of the RLL and $n_1 < 1$ in the FP, it results that $n_0 \neq n_1$ which causes the incident rays in the upper layer to be refracted. Thus, the closed-form profile of n_{eq} needs to be modified to obtain wave collimation in presence of the change of medium. By defining $\delta = n_0/n_1$, we can obtain an implicit expression of n_{eq} that provides an excellent collimation performance and reads as

$$\pi \ln\left(\frac{1+\sqrt{1-\eta^2}}{\eta}\right) + \sqrt{1-\eta^2}\left(\delta + \frac{\delta^3}{9}\left(\eta^2 + \frac{1}{2}\right)\right) + \pi \ln\rho = 0, \quad (1)$$

where $\eta = \rho n_{eq}/n_0$ and ρ is the radial component. As demonstrated also in [11], we can still generate a clean plane wave by placing the source in the inner focal region of the lens, which permits, in practice, total azimuthal scanning.

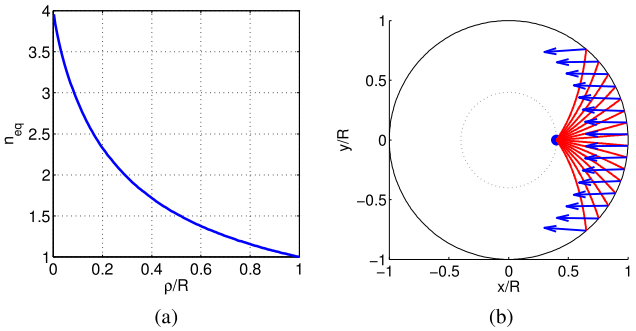

(a) (b)

Fig. 2. (a) Refractive index profile of the modified RLL to correct the refraction in the upper layer. (b) Ray trajectories (red lines) and direction of reflected and, subsequently, refracted rays (blue arrows).

In our case, we choose $\theta_0 = 54^o$ at the central frequency $f_0 = 30$ GHz by setting the FP height to $h_{FP} = 1.2(\lambda_0/4)$, so $n_1 = 0.81$. The refractive index profile estimated to account for the change of medium is shown in Fig. 2a, whereas the ray-paths (red lines) and the reflected ray directions in the FP region (blue arrows) illustrating the correction of the refraction are given in Fig. 2b. The position of the source is $\rho_s = 0.4R$, so it is to be observed that only the region inside $0.4R \leq \rho \leq R$ is finally implemented by the MTS and the maximum n_{eq} needed is 1.72 (see Fig. 2a).

IV. Design of Multi-beam Fabry-Perot Antenna

Fig. 1a shows the antenna structure. It has a radius of $R = 7\lambda_0$, where λ_0 is the free-space wavelength at f_0, and operates in the band $f \in [28, 32]$ GHz. The details of the dimensions for the bottom and top layers are given in Fig. 1b, where the PPW height is fixed to $h_{RLL} = 3.75$ mm. As a consequence, the antenna has a total diameter $D_{tot} = 147.5$ mm and an initially fixed total height $h_{tot} = 6.75$ mm. We employ open waveguides arranged in the inner focal region of the RLL to feed the lens in the bottom PPW [11]. As for the distribution of the ports, they are separated 22.5^o around ϕ, which ensures a mutual coupling between adjacent sources below -15 dB. As already mentioned, the plane wave generated by the RLL is transmitted to the upper layer through a corner reflector (Fig. 1b) that surrounds the structure. Then, an initial circular PPW section transmits the wave to the FP cavity, where a perforated top plate forms a PRS layer (see insets in Fig. 1a) which radiates the collimated field. By adjusting the diameter of the PRS holes, one can control the complex propagation constant and, hence, the pointing angle and the leakage constant [12]. Therefore, we fix the hole diameter to $d_{PRS} = 2.55$ mm to maintain the remaining not radiated power, i.e. the power returning to the lower layer, below -15 dB.

Fig. 3 presents the simulated directivity patterns in the E- and H-planes for one single excited port within the band of interest. Here, for a beam radiated at a given frequency, the E-plane is orthogonal to the xy-plane (see Fig. 1a) and it contains the origin and the direction of maximum directivity. The radiation properties in the E-plane are mostly determined by the FP cavity. Thereafter, the H-plane is orthogonal to the E-plane and contains the origin and the point of maximum radiation. The beam attributes in the H-plane are mainly given by the beam-forming structure. In this sense, the capacity of the RLL beam-former to keep the good performance within the 28-32 GHz band is noticeable, as observed in Fig. 3b. In addition, our proposed antenna provides a peak directivity larger than 24.5 dBi and an aperture efficiency greater than 40% within the operating band. The magnitude of the input reflection coefficient (not shown here) is below -10 dB for $f \in [28, 32]$ GHz and the total efficiency is above 90% in the same range of frequency. In turn, to demonstrate how the radiation performance can be replicated for any azimuthal direction, we show in Fig. 4 the simulated 3D directivity patterns (upper row) and the u-v color-maps (lower row) when

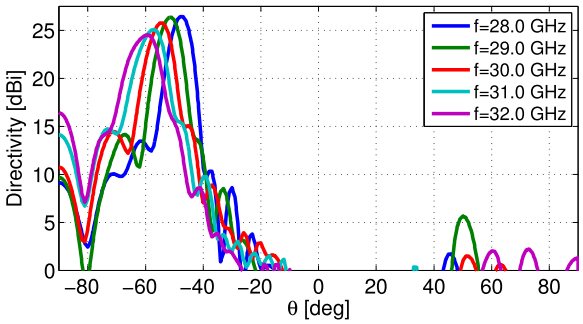

(a)

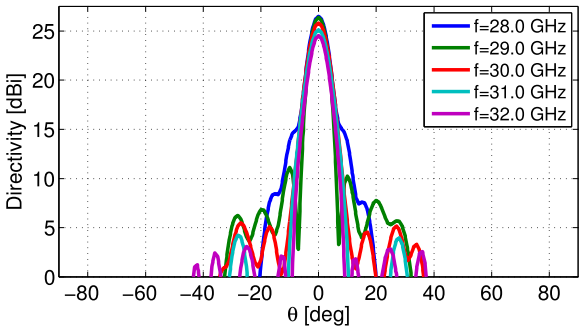

(b)

Fig. 3. Simulated directivity patterns obtained when only the port placed at $\phi = 0^o$ is activated at several frequencies within the operating band in the (a) E-plane and (b) H-plane.

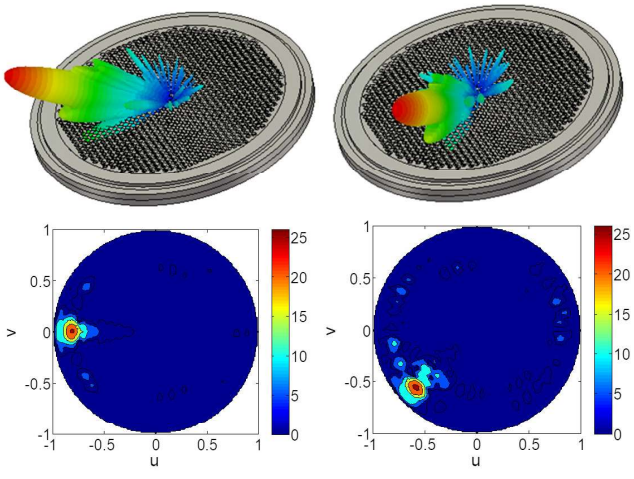

(a) (b)

Fig. 4. Simulated 3D directivity patterns (upper part) and u-v color-maps (lower part) in dBi at f_0 when the ports placed at (a) $\phi = 0^o$ and (b) $\phi = 45^o$ are excited.

switching between several ports at f_0. The port rotated by 45^o with respect to the x-axis is deliberately included since it involves the worst case in terms of the apparent periodicity of the corrugation pins and PRS holes regarding the direction of propagation of the plane wave.

As mentioned hereinabove, there exists also the possibility

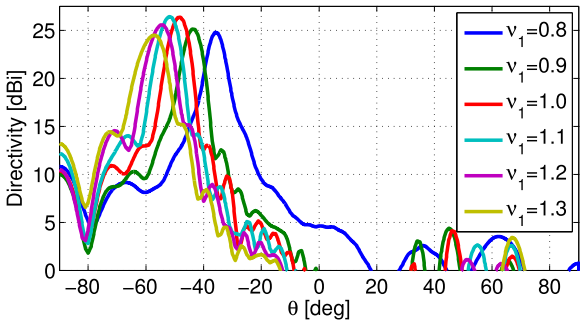

Fig. 5. Simulated E-plane directivity patterns at f_0 when the port placed at $\phi = 0^o$ is activated for different values of the FP height. The latter is defined here as $h_{FP} = \nu_1(\lambda_0/4)$.

of scanning in elevation by varying the height of the FP section. In practice, this can be attained by using piezoelectric materials or other mechanical configurations. Fig. 5 shows the scanning performance in the E-plane at f_0 when modifying the FP thickness h_{FP}. The patterns in the H-plane are almost not affected and we do not include them here for the sake of conciseness. For this particular case, it can be seen that the scanning range in elevation is $|\theta| \in [36^o, 58^o]$ and the scan losses remain below 2 dB. This kind of performance overcomes the constraint of using a modulated MTS [11] or a slotted plate [9], [16] as radiating aperture, since we achieve and independent control of θ and ϕ by combining port switching and the height variation of the FP cavity. Through the simultaneous activation of several ports, multiple beams can be also radiated at the same time.

V. Conclusion

We presented a low-profile metal-only Ka-band antenna with total azimuthal scanning by beam switching, which is also able to scan in elevation. The combination of a Reflecting Luneburg Lens (RLL) as beam-forming system and a Fabry-Perot (FP) cavity as radiating structure allows one to preserve the azimuthal symmetry. At the same time, the stacked configuration favors the compactness of the device, whereas a full-metal realization renders the losses in the structure negligible. The proposed antenna allows for an independent control of the elevation and azimuthal angles when scanning. Indeed, the direction of the beam in elevation can be controlled by varying the height of the FP and the azimuthal one by switching the ports arranged in the inner focal region of the RLL. Owing to its high-gain, 2D beam-steering performance and reduced form-factor, this solution is an excellent candidate for satellite communications in CubeSats and SmallSats.

Acknowledgment

The work of E. Martini and S. Maci was supported in part by the European Space Agency, under contract no. 4000127381/19/NL/AF, and in part by the Italian Ministry of University and Research, under the PRIN project "Metasurface Antennas for Satellite Applications". The work of J. Ruiz-García, C. Bilitos and D. González-Ovejero was funded in part by the European Union through the European Regional Development Fund (ERDF), and by the French Region of Brittany, Ministry of Higher Education and Research, Rennes Métropole and Conseil Départemental 35, through the CPER Project STIC & Ondes. They also received the support of the Agence de l'Innovation de Défense (AID) and the Conseil Régional de Bretagne.

References

[1] J. Wan, S. Lu, X. Wang, and Y. Ai, "A steerable spot beam reflector antenna for geostationary satellites," *IEEE Antennas Wireless Propag. Lett.*, vol. 15, pp. 89–92, May 2016.

[2] G. Han, B. Du, W. Wu, and B. Yang, "A novel hybrid phased array antenna for satellite communication on-the-move in Ku-band," *IEEE Trans. Antennas Propag.*, vol. 63, no. 4, pp. 1375–1383, Apr. 2015.

[3] N. Chahat *et al.*, "Advanced cubesat antennas for deep space and earth science missions: A review," *IEEE Antennas Propag. Mag.*, vol. 61, no. 5, pp. 37–46, Oct 2019.

[4] D. González-Ovejero, G. Minatti, G. Chattopadhyay, and S. Maci, "Multibeam by metasurface antennas," *IEEE Trans. Antennas Propag.*, vol. 65, no. 6, pp. 2923–2930, Jun. 2017.

[5] M. Faenzi *et al.*, "Metasurface antennas: New models, applications and realizations," *Sci. Rep.*, vol. 9, p. 10178, Jul. 2019.

[6] M. Bodehou, E. Martini, S. Maci, I. Huynen, and C. Craeye, "Multi-beam and beam scanning with modulated metasurfaces," *IEEE Trans. Antennas Propag.*, vol. 68, no. 3, pp. 1273–1281, Mar. 2020.

[7] O. Yurduseven, C. Lee, D. Gonzalez-Ovejero, M. Ettorre, R. Sauleau, G. Chattopadhyay, V. Fusco, and N. Chahat, "Multi-beam Si/GaAs holographic metasurface antenna at W-band," *IEEE Trans. Antennas Propag.*, pp. 1–1, 2020.

[8] M. U. Afzal, L. Matekovits, K. P. Esselle, and A. Lalbakhsh, "Beam-scanning antenna based on near-electric field phase transformation and refraction of electromagnetic wave through dielectric structures," *IEEE Access*, vol. 8, pp. 199 242–199 253, 2020.

[9] R. S. Hao, Y. J. Cheng, and Y. F. Wu, "Shared-aperture variable inclination continuous transverse stub antenna working at K- and Ka-bands for mobile satellite communication," *IEEE Trans. Antennas Propag.*, vol. 68, no. 9, pp. 6656–6666, Sep. 2020.

[10] A. H. Dorrah and G. V. Eleftheriades, "Peripherally excited phased array architecture for beam steering with reduced number of active elements," *IEEE Trans. Antennas Propag.*, vol. 68, no. 3, pp. 1249–1260, Mar. 2020.

[11] J. Ruiz-García, E. Martini, C. D. Giovampaola, D. González-Ovejero, and S. Maci, "Reflecting luneburg lenses," *IEEE Trans. Antennas Propag.*, vol. 69, no. 7, pp. 3924–3935, July 2021.

[12] A. T. Almutawa, A. Hosseini, D. R. Jackson, and F. Capolino, "Leaky-wave analysis of wideband planar Fabry–Pérot cavity antennas formed by a thick PRS," *IEEE Trans. Antennas Propag.*, vol. 67, no. 8, pp. 5163–5175, Aug 2019.

[13] K. A. Oyesina and A. M. H. Wong, "Metasurface-enabled cavity antenna: Beam steering with dramatically reduced fed elements," *IEEE Antennas Wireless Propag. Lett.*, vol. 19, no. 4, pp. 616–620, Apr. 2020.

[14] D. González-Ovejero, N. Chahat, R. Sauleau, G. Chattopadhyay, S. Maci, and M. Ettorre, "Additive manufactured metal-only modulated metasurface antennas," *IEEE Trans. Antennas Propag.*, vol. 66, no. 11, pp. 6106–6114, Nov 2018.

[15] ITU. "Radio Regulations 2020, Vol. I" (https://www.itu.int/pub/r-reg-rr-2020).

[16] A. Bhattacharyya, "Theory of beam scanning for slot array antenna excited by slow wave," *IEEE Antennas Propag. Mag.*, vol. 57, no. 2, pp. 96–103, Apr. 2015.